

Manipulating the momentum state of a condensate by sequences of standing-wave pulses

Wei Xiong, Xuguang Yue, Zhongkai Wang, Xiaoji Zhou,* and Xuzong Chen†
School of Electronics Engineering & Computer Science, Peking University, Beijing 100871, China

(Received 2 April 2011; published 11 October 2011)

We analyze the effects of sequences of standing-wave pulses on a Bose-Einstein condensate. The experimental observations are in good agreement with a numerical simulation based on band structure theory in an optical lattice. We also demonstrate that a coherent control method based on such a sequence of pulses is very efficient for the experimental design of specific momentum states.

DOI: [10.1103/PhysRevA.84.043616](https://doi.org/10.1103/PhysRevA.84.043616)

PACS number(s): 67.85.Hj, 67.85.Jk, 03.75.Kk

I. INTRODUCTION

Atomic interferometry is very useful in fundamental studies of coherence, decoherence, and phase shifts and for practical precision measurements, for example, gravimeters, gyroscopes, and gradiometers [1]. Atomic interferometry based on Bose-Einstein condensates (BECs) provides high contrasts, long integration times, and the possible use of small devices [2–4]. In such atomic interferometry, coherent momentum manipulation is very effective for splitting and recombining the condensate [5–7], hence realizing the interference. In some precision measurements, the accumulated phase is positively correlated with the atomic velocity, so that the larger is the atomic momentum, the more precise the measurements can be if the measuring time is unchanged.

The diffraction of atoms from standing-wave light, which is usually divided into three regimes, the Bragg, Raman-Nath, and channeling regimes [8], by the interaction intensity and duration, is one of the common methods to coherently manipulate the momentum states of a condensate [9–12]. One-pulse Bragg or Raman-Nath scattering can be applied for the preparation of momentum states, but those techniques are then limited by constraints on the pulse properties [8]. A momentum manipulation method by multipulse standing waves was proposed in [13], where the momentum states can be designed, but have not been observed yet, and the pulses are still restricted to the Raman-Nath regime.

In this paper, we apply a method for flexible manipulation of the atomic momentum states where the standing-wave pulses are less limited in pulse intensities and durations. Atomic diffraction from one, two, three, and four standing-wave pulses is demonstrated in our experiments and systematically analyzed by the band structure theory of a one-dimensional optical lattice. With this method, we are able to design and realize several specific momentum states, which may be applied in atomic interferometry. In principle, this method could be used for designing a wide range of possible target states.

This paper is organized as follows. In Sec. II, a theory to interpret the scattering process by a sequence of pulses is presented, where the standing wave is treated as a one-dimensional optical lattice. We derive a concise expression for calculating the probability of each momentum state at

the end of the process. In Sec. III, experiments with one-, two-, three-, and four-pulse scattering are demonstrated and compared to theoretical simulations. It is found that a correction due to momentum dispersion may be introduced into the theory for a better agreement with the experimental results. Section IV presents the experimental realization of several useful momentum states by coherent control. Section V contains discussion and conclusions.

II. THEORETICAL MODEL

We first consider a noninteracting condensate that is diffracted by a sequence of square-shaped standing-wave pulses with successive durations τ_i ($i = 1, 2, \dots, s + 1$), separated by the intervals τ_{fi} ($i = 1, 2, \dots, s$). The standing wave consists of a pair of laser beams detuned far enough to suppress spontaneous emission.

The periodic potential (one-dimensional optical lattice) [14,15] introduced by an ac Stark shift can be described as $V(x) = U_0 \cos^2(k_L x)$, with the trap depth U_0 and the laser's wave vector $k_L = 2\pi/\lambda_L$ (λ_L is the wavelength of the laser). The lattice leads to a band structure of the energy spectra, of which the eigenvalues of the energy $E_{n,q}$ and eigenvectors $|n,q\rangle$ (Bloch states) are labeled by the quasimomentum q and the band index n ; they satisfy the equation

$$\hat{H}|n,q\rangle = E_{n,q}|n,q\rangle, \quad (1)$$

where the Hamiltonian $\hat{H} = \hat{p}^2/2M + U_0 \cos^2(k_L x)$, with the atomic momentum \hat{p} and the atomic mass M . The Bloch states form a quasimomentum space. In the lattice, the spatial periodicity of the wave function results in separated peaks in momentum space, corresponding to the reciprocal lattice vector $2k_L$.

When a condensate with an initial momentum $p_{m_0} = \hbar(q + 2m_0 k_L)$ (\hbar is the Plank constant, $-k_L \leq q \leq k_L$, $m_0 = \dots, -1, 0, 1, \dots$) is abruptly loaded into a lattice, the wave packet can be described as a superposition of Bloch states:

$$|\Psi(t=0)\rangle = \sum_{n=0}^{\infty} |n,q\rangle \langle n,q|p_{m_0}\rangle, \quad (2)$$

where $\langle n,q|p_{m_0}\rangle = c_{n,q}(m_0)$. The n th Bloch state evolves independently as $e^{-iE_{n,q}t/\hbar}$, and the total wave function evolves as

$$|\Psi(t)\rangle = \sum_{n=0}^{\infty} c_{n,q}(m_0) e^{-iE_{n,q}t/\hbar} |n,q\rangle. \quad (3)$$

*xjzhou@pku.edu.cn

†xuzongchen@pku.edu.cn

When the incident light is switched off after the duration τ_1 , the wave function is projected back to the momentum space from the quasimomentum space. The coefficient $b(m_0, m, \tau_1)$ of each $|p_m\rangle$ state ($m = \dots, -1, 0, 1, \dots$) can be found as

$$b(m_0, m, \tau_1) = \sum_{n=0}^{\infty} c_{n,q}(m_0) c_{n,q}(m) e^{-iE_{n,q}\tau_1/\hbar}. \quad (4)$$

For a zero initial momentum of the condensate, the subscript q can be omitted for simplification, and $m_0 = 0$. For one-pulse scattering, the population of the $|p_m\rangle$ state is $P_m^{(1)} = |b(0, m, \tau_1)|^2$. It can be seen that the probabilities of the momentum states after one scattering pulse depend on the lattice depth and the pulse duration. The lattice depth determines the band structure and is reflected in the terms $c_{n,q}$. The pulse duration influences the phase evolution of each Bloch state as $e^{-iE_{n,q}\tau_1/\hbar}$.

A multipulse process that consists of a number of single pulses and intervals can be solved as follows. The wave function of the condensate after the first pulse τ_1 can be derived from Eq. (4) as

$$|\Psi(\tau_1, t)\rangle = \sum_m b(m_0, m, \tau_1) e^{-iE^{(m)}t/\hbar} |2m\hbar k_L\rangle. \quad (5)$$

After the first interval τ_{f1} and the second pulse τ_2 , the population of the $|p_m\rangle$ state is

$$P_m^{(2)} = \left| \sum_{m_1} b(m_0, m_1, \tau_1) e^{-iE^{(m_1)}\tau_{f1}/\hbar} b(m_1, m, \tau_2) \right|^2. \quad (6)$$

As shown in Eq. (6), the population is affected by the two pulses, the first one corresponding to $b(m_0, m_1, \tau_1)$ and the second to $b(m_1, m, \tau_2)$. During the interval τ_{f1} , the phase of the $|p_{m_1}\rangle$ state evolves through time as $e^{-iE^{(m_1)}t/\hbar}$, where $E^{(m_1)} = (2m_1\hbar k_L)^2/2M = 4m_1^2 E_R$ is the kinetic energy, and $E_R = (\hbar k_L)^2/2M$ is the single-photon recoil energy. The interval τ_{f1} produces a phase shift $e^{-iE^{(m_1)}\tau_{f1}/\hbar}$ and contributes to the momentum distribution.

In the same way, the population of the $|p_m\rangle$ state after $(s+1)$ pulses is

$$P_m^{(s+1)} = \left| \sum_{m_1, m_2, \dots, m_s} \prod_{i=1}^{s+1} b(m_{i-1}, m_i, \tau_i) \prod_{i=1}^s e^{-iE^{(m_i)}\tau_{f_i}/\hbar} \right|^2 \quad (7)$$

with $m_0 = 0$, and $m_{s+1} = m$.

From the analysis above, the momentum distribution after scattering of a sequence of pulses is influenced by not only the lattice pulses with the term $\prod_{i=1}^{s+1} b(m_{i-1}, m_i, \tau_i)$, but also the intervals among the pulses as reflected in the term $\prod_{i=1}^s e^{-iE^{(m_i)}\tau_{f_i}/\hbar}$. Although the populations of the momentum states do not change during the intervals, the phase-evolution rates of the momentum states with different kinetic energies are not identical. The phase deviations between the states oscillate from 0 to 2π with the interval, and the heterogeneously accumulated phases change the distribution of the condensate in the quasimomentum space.

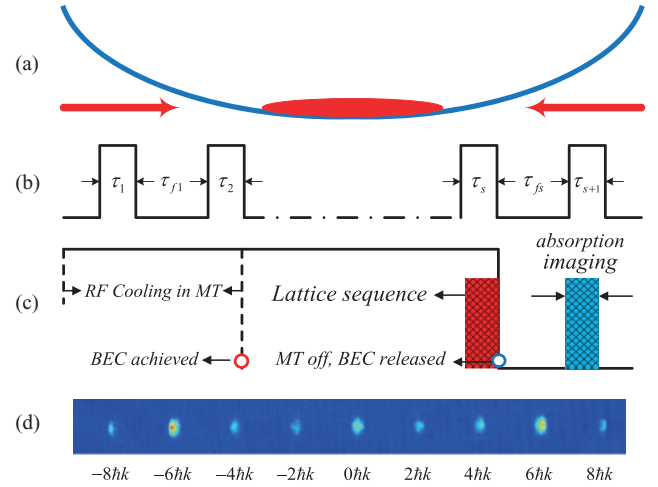


FIG. 1. (Color online) (a) A pair of counterpropagating light beams applied to a condensate in magnetic trap. (b) The scattering process: a sequence of standing-wave pulses, containing s intervals with widths τ_{f_i} ($i = 1, 2, \dots, s$) and $s+1$ light pulses with durations τ_i ($i = 1, 2, \dots, s+1$). The incident light's wavelength is 852 nm and its maximum intensity can reach $120E_R$. (c) The procedure for the experiments. The condensate is exposed to a sequence of standing-wave pulses and then released from the magnetic trap. The absorption images of the condensate can be observed after the free fall. (d) A TOF signal obtained in our experiment.

III. EXPERIMENTS WITH STANDING-WAVE PULSE SEQUENCES

We performed experiments on a condensate in a magnetic trap (MT) [see Fig. 1(a)] being scattered by a sequence of standing-wave pulses [see Fig. 1(b)]. As shown in Fig. 1(c), after precooling, a cigar-shaped ^{87}Rb condensate of 2×10^5 atoms in the $5^2S_{1/2} |F=2, M_F=2\rangle$ state was achieved by radio frequency (rf) cooling in the magnetic trap, of which the axial frequency is 20 Hz and the radial frequency 220 Hz [16,17]. A pair of counterpropagating laser beams, of which the durations were controlled by an acousto-optical modulator and the amplitudes adjusted by the injection current of a tapered amplifier, were applied to the condensate along the axial direction. The linearly polarized incident light at wavelength $\lambda_L = 852$ nm was focused with a waist of $110 \mu\text{m}$ to cover the condensate. The trap depth, which was calibrated experimentally by Kapitza-Dirac scattering, reached $120E_R$, corresponding to a light power of 320 mW. The incident light and the magnetic trap were simultaneously shut after the BEC-light interaction. After 30 ms free falling and ballistic expansion, the atomic gas was pictured by absorption imaging. Since the minimum gap between different momentum states is $2\hbar k$, which is much larger than the momentum width of a single momentum state, the components with different momenta will be separated in the time of flight (TOF) signal [see Fig. 1(d)], and it is possible to read the atomic number of each momentum state separately as N_m (the momentum order $m = \dots, -2, -1, 0, 1, 2$). The relative population of the momentum state $|2m\hbar k\rangle$ can be evaluated as $N_m / \sum N_m$.

The lattice in our experiments is quite deep, so we concentrate on the short-pulse diffractions to avoid the decoherence

and heating effects of long pulses relevant for Bragg scattering. However, for more flexible momentum manipulation, our pulses are not so short as the Raman-Nath pulses [18] used in previous works.

A brief introduction to the Raman-Nath regime is given in the following for comparison. In the scattering process, the evolution during the free-evolution intervals is analyzed as in the previous section, while the effect of the lattice with adequately short duration τ can be analytically solved by use of the Schrödinger equation $i\hbar\partial|\Psi(t)\rangle/\partial t = \hat{H}|\Psi(t)\rangle$, after omission of the atomic kinetic energy term $\hat{p}^2/2M$ in the Hamiltonian. This approximation can be made when the displacement of the scattered atoms during the interaction time is much smaller than the spatial period of the standing wave. Equivalently, the standing-wave duration τ and the single-photon recoil frequency $\omega_r = \hbar k_L^2/2M$ have to satisfy $\tau \ll 1/\omega_r$. The pulse is able to split a stationary condensate into components with symmetrical momenta $p_n = 2n\hbar k_L$ ($n = 0, \pm 1, \pm 2, \dots$), with corresponding populations $P_n = J_n^2(U_0\tau/2\hbar)$, where $J_n(z)$ are Bessel functions of the first kind.

First we demonstrate a one-pulse scattering experiment. A condensate is exposed to a standing-wave pulse with depth $100E_R$ and duration varying from 0 to $30\ \mu\text{s}$. The relative populations of the condensates with momenta $0\hbar k$, $\pm 2\hbar k$, $\pm 4\hbar k$, and $\pm 6\hbar k$, corresponding to Figs. 2(a)–2(d), respectively, are measured and theoretically analyzed. In addition, the theoretical analysis with the Raman-Nath approximation is also shown in the figure for comparison. It can be seen that within $3\ \mu\text{s}$ the theoretical analysis with the Raman-Nath approximation (blue solid line) is close to the experimental results (black dots), and so is the theoretical analysis with band structure theory (red dashed line). When the pulse duration exceeds $3\ \mu\text{s}$, the analysis with the Raman-Nath approximation gradually goes far away from the experimental results, while the numerical simulation with band structure

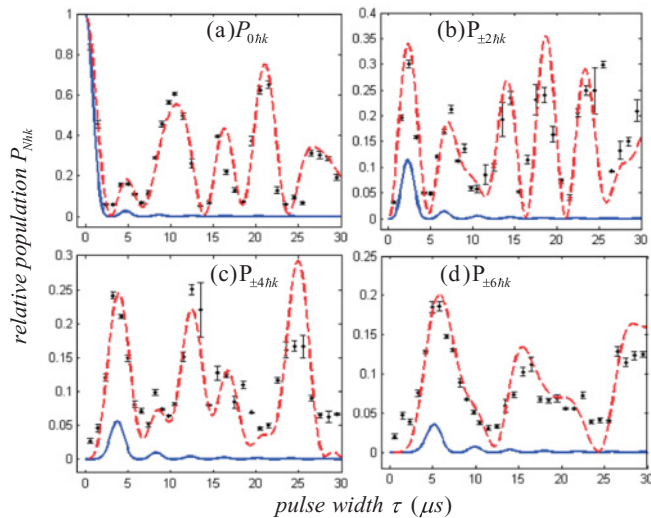


FIG. 2. (Color online) Single-pulse scattering of condensate: The black dots represent the experiment results. The blue solid line is the theoretical analysis with the Raman-Nath approximation. The red dashed line is the numerical simulation with band structure theory. (a)–(d) correspond to relative populations of the condensates with momenta $0\hbar k$, $\pm 2\hbar k$, $\pm 4\hbar k$, and $\pm 6\hbar k$, respectively.

theory still agrees with the experimental results throughout the entire time scale. As shown in Fig. 2, the probability of each momentum state oscillates with the pulse duration as described by the band structure theory. It is clear that, in the single-pulse scattering process, the band structure theory works well not only for the short pulse but also for the longer pulse, because the atomic motion has been taken into account. So the atomic diffraction by a single standing-wave pulse can be predicted in a wider range of pulse duration with the band structure theory.

Then we increase the number of pulses in the experiments to explore the extra factors influencing the momentum distributions. Two groups of experiments are carried out, one consisting in two two-pulse sequences and the other using a train of three or four pulses. In every sequence, all the pulses are the same and all the intervals are identical to make the experiments more convenient to carry out. For further comparison between the band structure theory and the analysis in the Raman-Nath regime, every single pulse is made short enough for the Raman-Nath approximation.

Two experiments with two-pulse scattering are demonstrated in Fig. 3, in which the relative populations of the stationary condensate $P_{0\hbar k}$ are shown versus the varied intervals τ_f . The parameters of the scattering pulses used in different sequences are chosen to be the same products of the lattice depth and the pulse duration, so that each pulse affects the condensate equivalently. As shown in the figure,

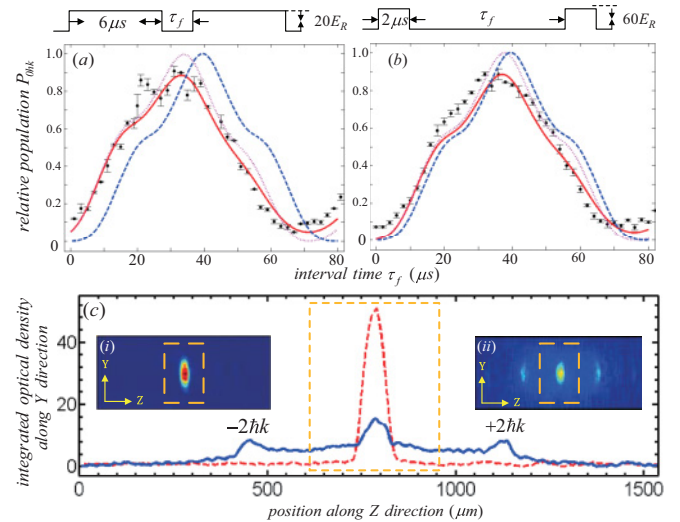


FIG. 3. (Color online) Two-pulse scattering of the condensate: The relative populations of the stationary condensate, $P_{0\hbar k}$, versus the varied intervals τ_f . The parameters of the experiments are described above each figure. The black dots are the experimental results. The blue dashed line is the analysis with the Raman-Nath approximation. The magenta dotted line is the numerical simulation with band structure theory. The red solid line is a numerical simulation taking into account the momentum dispersion. (c) A demonstration of momentum expansion introduced by s -wave scattering. The TOF signal (i) corresponds to the dashed curve and pictures the momentum distribution before the lattice pulse. The signal (ii) corresponds to the solid curve and shows the momentum distribution after the pulse. The momentum width along the Z direction (the lattice direction) is evaluated based on the parts in the dashed boxes which include the momenta from $-\hbar k$ to $\hbar k$.

the intervals actually affect the final momentum distribution, and the theoretical analysis with the band structure theory and Raman-Nath approximation both picture well the evolution of the atomic distributions versus the interval between the two pulses. The results for two-pulse scattering can be explained as follows: Since the phase shift accumulated during the interval varies harmonically from 0 to 2π , the probability of the stationary condensate oscillates between the minimum and the maximum. When the phase shift is 2π with the interval $\pi\hbar/2E_R$ (around $80\ \mu\text{s}$), the wave function is little affected by the interval and the two pulses diffract the condensate as one combined pulse to make the probability $P_{0\hbar k}$ the minimum. When the phase shift is π with the interval $\pi\hbar/4E_R$ (about $40\ \mu\text{s}$), the second pulse produces an effect opposite to that of the first one, diffracting the nonstationary components of the condensate back to the stationary one and making the probability $P_{0\hbar k}$ the maximum.

It also can be seen from Fig. 3 that the numerical simulation with band structure theory is much closer to the experimental results than the analytical solution with the Raman-Nath approximation. It is conjectured that the phase evolution during the scattering process makes the difference. The phase evolution in the scattering process is neglected in the Raman-Nath approximation, but not in the numerical simulation with band structure theory. Although the duration of the scattering process is short, the phase shifts in the scattering process still increase. The phase shift in the scattering process needs to be taken into account and influences the final momentum distribution. As a result, the longer is the scattering pulse, the larger is the difference. Although the maximum of the probability $P_{0\hbar k}$ corresponds to the interval $\pi\hbar/4E_R$, the two-pulse experiments in Fig. 3 clearly show that the longer pulse leads to a larger difference. In Fig. 3(a), the pulse duration is $6\ \mu\text{s}$, and the probability $P_{0\hbar k}$ reaches a maximum with the interval $34\ \mu\text{s}$. In Fig. 3(b), the pulse duration is $2\ \mu\text{s}$, the probability $P_{0\hbar k}$ gets to its maximum with the interval $38\ \mu\text{s}$.

Nevertheless, there is still some obvious deviation between the simulation and the experimental results. It is observed that the momentum width has expanded after the previous pulse [see Fig. 3(c)], because of the s -wave scattering between the different momentum states. Consequently, this dispersion process is approximated to an initial momentum width of $\sim 0.1\hbar k_L$ on average to optimize the numerical simulation. Unlike the analysis without momentum width, the phase evolution is different for different initial momenta and this results in a phase dispersion. The quasimomentum modes obtained at the end of the diffraction process result from the linear superposition of final states obtained after time evolution of the different momenta populating the initial BEC. It can be seen from Fig. 3 that the approximation is effective.

As discussed in [19], the maximum of the probability $P_{0\hbar k}$ will never reach 1 thanks to the imperfect optical lattice. In our case, the momentum expansion is an explanation of the similar situation as shown in Fig. 3. Since the momentum width is considered, the phase shift is populated around π with a certain width, instead of a definite π , with the interval $\pi\hbar/4E_R$. In other words, there is no interval that accumulates a phase shift exactly equal to π , so with any interval, the second standing-wave pulse is not able to diffract all the condensates back to the stationary part.

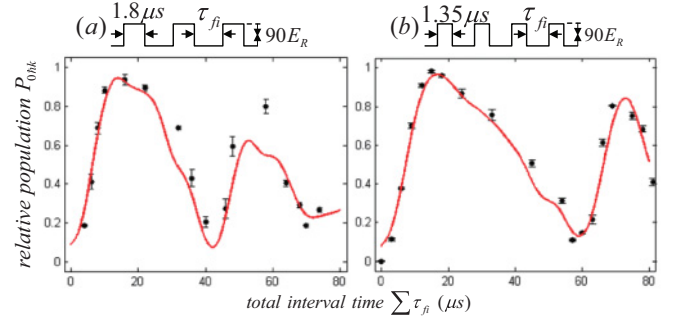


FIG. 4. (Color online) Three-pulse and four-pulse scattering of the condensate: The relative populations of the stationary condensate $P_{0\hbar k}$ versus the varied total intervals $\sum \tau_{fi}$. The parameters of the experiments are described above each figure. The black dots are the experimental results. The red solid line is a numerical simulation taking into account the momentum dispersion.

The experiments with one three-pulse and one four-pulse scattering are demonstrated in Fig. 4, where the relative populations of the stationary condensate $P_{0\hbar k}$ are shown versus the varied total intervals $\sum \tau_{fi}$. In each experiment, the total interaction intensity $\sum U_0\tau$ is the same, with different numbers of pulses. These two experiments show that, although the total interactions and intervals are the same, the different processes of phase accumulation in the two kinds of pulse sequence result in distinct momentum distributions. We directly apply the band structure theory with momentum dispersion to analyze the experiments in Fig. 4, and the corrected simulations agree with the experiments quite well.

IV. MANIPULATION OF THE MOMENTUM STATES AS DESIGN

The experiments and numerical simulations above have shown the possibility and feasibility of the manipulation of a condensate's momentum states. We managed to design several two-pulse sequences to achieve high-contrast momentum states such as $|\pm 2\hbar k\rangle$, $|\pm 4\hbar k\rangle$, and $|\pm 6\hbar k\rangle$, which may be useful in atomic interferometry [20,21]. For each state, we apply two totally different two-pulse sequences to show the flexibility of the method. The general method to achieve the target states is to find the condition of the minimum of the square deviation $\Delta^2 = \sum_{m=-\infty}^{+\infty} (P_m^g - P_m)^2$, where P_m^g is the probability of $|2m\hbar k_L\rangle$ in the goal state, and P_m is that generated by the sequence. A second method, as the target is to obtain the highest population of some particular momentum state, consists in scanning the set of initial conditions and choosing the one corresponding to the maximum value of the desired population. We apply the two methods above separately and obtain the same pulse sequences. As shown in Fig. 5, the experimental results (the black circles) agree well with the expectations of the designs (the blue diamonds), whether the pulses are in the Raman-Nath regime [see Fig. 5(b)] or not (see the other panels in Fig. 5). When the momentum dispersion is being considered, the expected momentum distributions (the red squares) get closer to the experimental values; note that the figures only display the relative populations of the target states and omit the others for clarity.

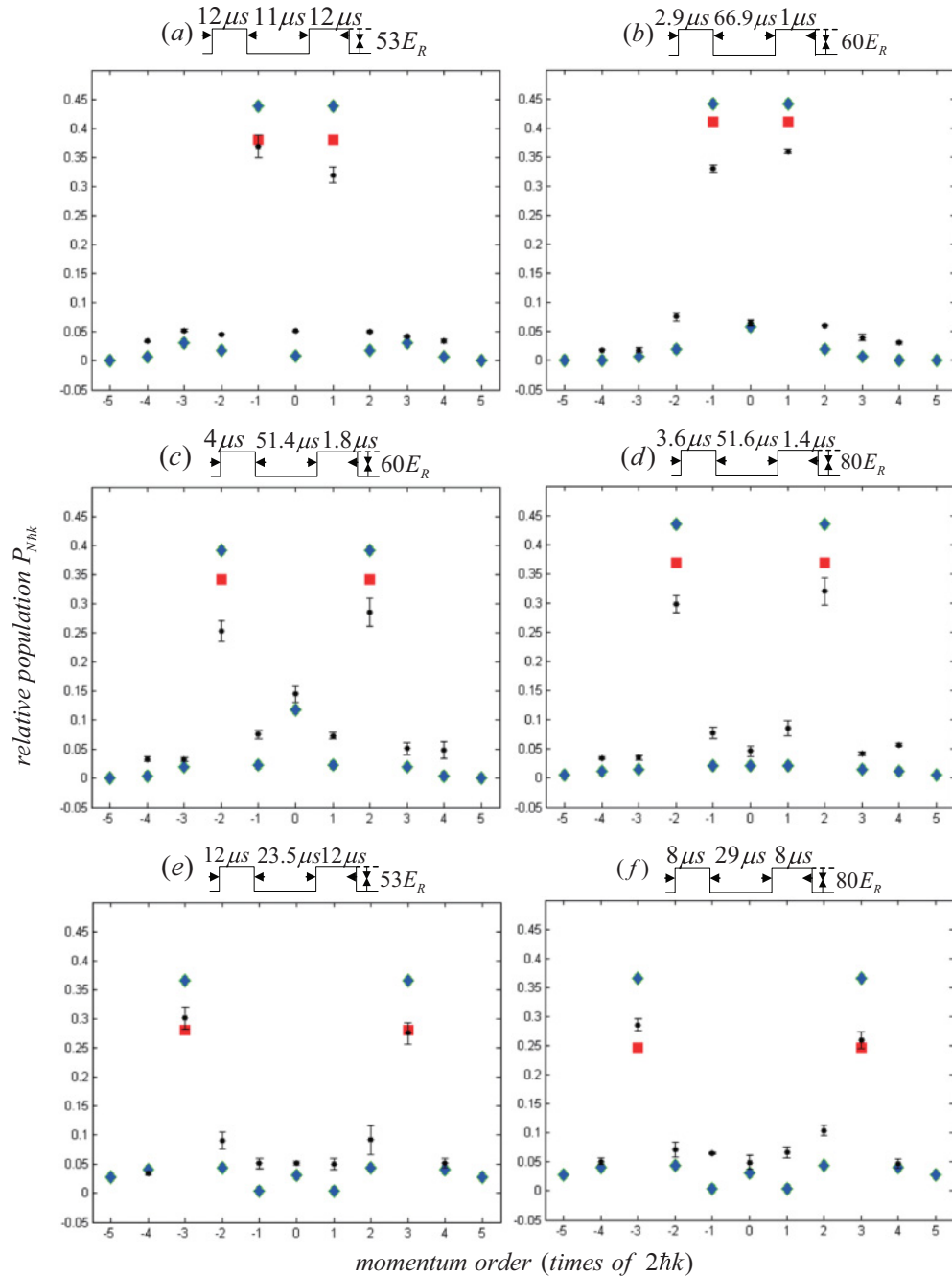


FIG. 5. (Color online) Experimental realization of designed momentum states. The expected momentum state is $\pm 2\hbar k_L$ [(a) and (b)], $\pm 4\hbar k_L$ [(c) and (d)], and $\pm 6\hbar k_L$ [(e) and (f)]. The pulse sequences are shown above each figure. The black circles are experimental results. The blue diamonds are the expectations based on the design. The red squares are the modified design with momentum width included, which agree better with the experiments.

It can be seen from Fig. 5 that the momentum width correction can improve the precision of prediction with our method. The average relative deviation between the experimental results and the expected values without inclusion of the momentum width is 25.03%, while the deviation is decreased to 13.15% with the correction.

An asymmetry of the momenta can be observed in Fig. 5, and it may be ascribed to the following factors. Besides the measurement error, there is an imperfection of the standing wave, brought forth by the unbalanced intensity of the laser

beams. External field fluctuations (as in the magnetic trap) during the scattering process may also affect the momentum distribution.

V. DISCUSSION AND CONCLUSIONS

Band structure theory is a global method to deal with standing-wave scattering by a condensate, while Bragg and Raman-Nath scattering are two special situations which can be analytically solved with their respective approximations.

In the Bragg regime, the potential height introduced by the standing wave is restrained below $4E_R$ and that leads to a difficulty in generating higher-order momentum states. In the Raman-Nath regime, the intensity of the standing wave is not limited so that higher-order momentum states can be generated symmetrically [22,23]. However, the pulse duration has to be short enough for the atomic motion to be neglected, so the momentum states cannot be predicted in this regime if the pulse duration is slightly longer. In our work, the scattering can be well explained and numerically analyzed within a much wider range of pulse intensity and duration. So it is natural that more momentum states can be generated.

In our paper, we compared the scattering by one pulse and that by a train of pulses. Some valuable states, such as $|\pm 2\hbar k\rangle$, $|\pm 4\hbar k\rangle$, and $|\pm 6\hbar k\rangle$ states with high contrast, cannot be realized by single-pulse scattering, while they can be realized by a sequence of standing-wave pulses. A sequence of lattice pulses is a more effective and flexible tool for momentum manipulation. It can generate many useful momentum states, in addition to the ones demonstrated in our work. In the future, more parameters could be changed to obtain better results in design of states.

Although the numerical simulation is corrected to take into account the momentum dispersion, some deviations between the experiments and the simulation still exist. The inaccuracy of the lattice-depth calibration, which is 5% at least, is one of

the reasons. The phase shift introduced by the magnetic trap is another one, although its influence is estimated to be within 0.03%, which is below the experimental uncertainty. The heating and momentum exchange during the s -wave scattering may also lead to some differences, which need further study.

In conclusion, we developed a method for more flexible manipulation of the condensate's momentum states, where the momentum states can be controlled by standing-wave pulses in a wider range of pulse intensity, duration, or quantity. Experiments in which a condensate is scattered by a sequence of standing-wave pulses are demonstrated. A global theory, treating the standing wave as an optical lattice, is applied to explain the experiments. With this theory, we are able to design pulse sequences for realizing states such as $|\pm 2\hbar k\rangle$, $|\pm 4\hbar k\rangle$, and $|\pm 6\hbar k\rangle$ and experimentally realize them, which may be applied in atomic interferometry to improve measurement precision.

ACKNOWLEDGMENTS

We would like to thank Thibault Vogt for critical reading of our paper. This work is supported by the National Fundamental Research Program of China under Grant No. 2011CB921501 and the National Natural Science Foundation of China under Grants No. 61027016, No. 61078026, No. 10874008, and No. 10934010.

-
- [1] Alexander D. Cronin *et al.*, *Rev. Mod. Phys.* **81**, 1051 (2009).
 - [2] Y. Torii, Y. Suzuki, M. Kozuma, T. Sugiura, T. Kuga, L. Deng, and E. W. Hagley, *Phys. Rev. A* **61**, 041602 (2000).
 - [3] R. E. Sapiro, R. Zhang, and G. Raithel, *Phys. Rev. A* **79**, 043630 (2009).
 - [4] F. Baumgartner, R. J. Sewell, S. Eriksson, I. Llorente-Garcia, J. Dingjan, J. P. Cotter, and E. A. Hinds, *Phys. Rev. Lett.* **105**, 243003 (2010).
 - [5] L. Deng, E. W. Hagley, J. Denschlag, J. E. Simsarian, M. Edwards, C. W. Clark, K. Helmerson, S. L. Rolston, and W. D. Phillips, *Phys. Rev. Lett.* **83**, 5407 (1999).
 - [6] M. Kozuma, L. Deng, E. W. Hagley, J. Wen, R. Lutwak, K. Helmerson, S. L. Rolston, and W. D. Phillips, *Phys. Rev. Lett.* **82**, 871 (1999).
 - [7] Y. B. Ovchinnikov, J. H. Muller, M. R. Doery, E. J. D. Vredenburg, K. Helmerson, S. L. Rolston, and W. D. Phillips, *Phys. Rev. Lett.* **83**, 284 (1999).
 - [8] C. Keller *et al.*, *Appl. Phys. B* **69**, 303 (1999).
 - [9] S. Gupta *et al.*, *C. R. Acad. Sci., Ser. IV: Phys., Astrophys.* **2**, 479 (2001).
 - [10] D. E. Pritchard *et al.*, *Ann. Phys. (Berlin)* **10**, 35 (2001).
 - [11] P. Meystre, *Atom Optics* (Springer, New York, 2001).
 - [12] S. Wu, Y. J. Wang, Q. Diot, and M. Prentiss, *Phys. Rev. A* **71**, 043602 (2005).
 - [13] M. Edwards, B. Benton, J. Heward, and C. W. Clark, *Phys. Rev. A* **82**, 063613 (2010).
 - [14] O. Morsch *et al.*, *Rev. Mod. Phys.* **78**, 179 (2006).
 - [15] J. H. Denschlag *et al.*, *J. Phys. B* **35**, 3095 (2002).
 - [16] F. Yang, X. Zhou, J. Li, Y. Chen, L. Xia, and X. Chen, *Phys. Rev. A* **78**, 043611 (2008).
 - [17] X. J. Zhou, F. Yang, X. Yue, T. Vogt, and X. Chen, *Phys. Rev. A* **81**, 013615 (2010).
 - [18] J. H. Huckans, I. B. Spielman, B. Laburthe Tolra, W. D. Phil, and J. V. Porto, *Phys. Rev. A* **80**, 043609 (2009).
 - [19] K. Li, L. Deng, E. W. Hagley, M. G. Payne, and M. S. Zhan, *Phys. Rev. Lett.* **101**, 250401 (2008).
 - [20] S. Beattie, B. Barrett, I. Chan, C. Mok, I. Yavin, and A. Kumarakrishnan, *Phys. Rev. A* **80**, 013618 (2009).
 - [21] B. Rohwedder, *Eur. Phys. J. D* **13**, 255 (2001).
 - [22] R. E. Sapiro, R. Zhang, and G. Raithel, *New J. Phys.* **11**, 013013 (2009).
 - [23] B. Gadway *et al.*, *Opt. Express* **17**, 19173 (2009).